

APOLLO: An Adaptive Parameter-wise Diagonal Quasi-Newton Method for Nonconvex Stochastic Optimization

Xuezhe Ma*

*Information Sciences Institute
University of Southern California*

XUEZHEMA@ISI.EDU

Abstract

In this paper, we introduce APOLLO, a quasi-Newton method for nonconvex stochastic optimization, which dynamically incorporates the curvature of the loss function by approximating the Hessian via a diagonal matrix. Importantly, the update and storage of the diagonal approximation of Hessian is as efficient as adaptive first-order optimization methods with linear complexity for both time and memory. To handle nonconvexity, we replace the Hessian with its rectified absolute value, which is guaranteed to be positive-definite. Experiments on three tasks of vision and language show that APOLLO achieves significant improvements over other stochastic optimization methods, including SGD and variants of Adam, in terms of both convergence speed and generalization performance. The implementation of the algorithm is available at <https://github.com/XuezheMax/apollo>.

1. Introduction

Nonconvex stochastic optimization is of core practical importance in many fields of machine learning, in particular for training deep neural networks (DNNs). First-order gradient-based optimization algorithms, conceptually attractive due to their linear efficiency on both the time and memory complexity, have led to tremendous progress and impressive successes. A number of advanced first-order algorithms have emerged over the years to pursue fast and stable convergence, among which stochastic gradient descent (SGD) (Robbins and Monroe, 1951; LeCun et al., 1998), equipped with momentum (Rumelhart et al., 1985; Qian, 1999; Bottou and Bousquet, 2008), has stood out for its simplicity and effectiveness across a wide range of applications (Hinton and Salakhutdinov, 2006; Hinton et al., 2012; Graves, 2013). However, one disadvantage of SGD is that the gradients in different directions are scaled uniformly, resulting in limited convergence speed and sensitive choice of learning rate, and thus has spawned a lot of recent interest in accelerating SGD from the algorithmic and practical perspectives.

Recently, many *adaptive* first-order optimization methods have been proposed to achieve rapid training progress with element-wise scaled learning rates, and we can only mention a few here due to space limits. In their pioneering work, Duchi et al. (2011) proposed AdaGrad, which scales the gradient by the square root of the accumulative square gradients from the first iteration. While AdaGrad works well for sparse settings, its performance significantly degrades for dense settings, primarily due to the monotonic increase of the accumulation. Subsequently, several methods have been proposed with the intuition to limit the accumulation to a small

*. Work was done at Carnegie Mellon University.

window of past iterations, and in particular exponentially reduce the weight of earlier iterations. Notable works incorporating this method are RMSProp (Tieleman and Hinton, 2012), AdaDelta (Zeiler, 2012), and Adam (Kingma and Ba, 2015), among which Adam has become the default optimization algorithm across many deep learning applications because of its fast convergence speed and relatively consistent selections of hyper-parameters (Ruder, 2016; Zhang et al., 2020). However, it has been observed that these adaptive optimization methods may converge to bad/suspicious local optima, resulting in worse generalization ability than their non-adaptive counterparts (Wilson et al., 2017), or fail to converge due to unstable and extreme learning rates (Luo et al., 2019).

Quasi-Newton methods have been widely used in solving convex optimization problems, due to their efficient computation and fast convergence rate (Broyden, 1967; Dennis and Moré, 1977). However, the stochastic, high-dimensional and nonconvex nature of many machine learning tasks, such as training deep neural networks, has rendered many classical quasi-Newton methods ineffective and/or inefficient (Keskar and Berahas, 2016; Wang et al., 2017; Yao et al., 2020). Indeed, in many natural language processing (NLP) and computer vision (CV) tasks (He et al., 2016; Ma and Hovy, 2016; Luo et al., 2019), SGD (with momentum) is chosen as the optimizer, benefiting from its stable and efficient training and outstanding generalization.

In this work, we develop APOLLO, a quasi-Newton method for nonconvex stochastic optimization to simultaneously tackle the aforementioned challenges of stochastic variance, nonconvexity and inefficiency. Algorithmically, APOLLO dynamically incorporates the curvature of the objective function with diagonally approximated Hessian. It only requires first-order gradients and updates the approximation of the Hessian diagonally so that it satisfies a parameter-wise version of the weak secant condition (Wolfe, 1959). To handle nonconvexity, we replace the Hessian with its rectified absolute value, the computation of which is also efficient under our diagonal approximation, yielding an efficient optimization algorithm with linear complexity for both time and memory (§3). Experimentally, through three tasks on CV and NLP with popular deep neural networks, including ResNets (He et al., 2016), LSTMs (Hochreiter and Schmidhuber, 1997) and Transformers (Vaswani et al., 2017), we demonstrate that APOLLO significantly outperforms SGD and variants of Adam, in terms of both convergence speed and generalization performance (§4).

2. Backgrounds

In this section, we set up the notations on nonconvex stochastic optimization, briefly review the (quasi-) Newton methods, and discuss the problems of applying quasi-Newton methods to nonconvex stochastic optimization that we attempt to study in the rest of the paper.

2.1 Nonconvex Stochastic Optimization

In this paper, we consider the following nonconvex stochastic optimization problem:

$$\min_{\theta \in \mathcal{R}^d} f(\theta) = \mathbb{E}[l(\theta; \Gamma)] \quad (1)$$

where $l : \mathcal{R}^d \times \mathcal{R}^n \rightarrow \mathcal{R}$ is a continuously differentiable (and possibly nonconvex) function, $\theta \in \mathcal{R}^d$ denotes the parameter to be optimized, $\Gamma \in \mathcal{R}^n$ denotes a random variable with distribution function P , and $\mathbb{E}[\cdot]$ denotes the expectation w.r.t Γ . Intuitively, Γ incorporates

noises in f , leading to a stochastic objective function. A special case of (1) that arises frequently in machine learning is the empirical risk minimization problem:

$$\min_{\theta \in \mathcal{R}^d} f(\theta) = \frac{1}{N} \sum_{i=1}^N l_i(\theta) \quad (2)$$

where $l_i : \mathcal{R}^d \rightarrow \mathcal{R}$ is the loss function corresponds to the i -th data, and N is the number of data samples that is assumed to be extremely large. Objective functions may also have other sources of noise than data subsampling, such as dropout (Srivastava et al., 2014) in deep neural networks.

Decoupled Parameters. In this work, we consider a setting of decoupled parameters: $\theta = \{\theta^{(l)}, l = 1, \dots, L\}$. Intuitively, under this setting the parameter θ is decoupled into a sequence of parameters serving different functionalities. For example, in neural network training the parameters of a neural network can be naturally decoupled into the parameters of different layers or modules.

2.2 Newton and quasi-Newton Methods

Newton's method usually employs the following updates to solve (1):

$$\theta_{t+1} = \theta_t - H_t^{-1} g_t \quad (3)$$

where $g_t = \nabla f(\theta_t)$ is the gradient at θ_t and $H_t = \nabla^2 f(\theta_t)$ is the Hessian matrix. The convergence rate of Newton's method is *quadratic* under standard assumptions (Nocedal and Wright, 2006). However, major challenges with this method are i) the expensive computation of the inverse Hessian at every iteration and the corresponding quadratic memory complexity; and ii) the limitation to convex functions (nonconvexity results in negative curvature of H_t and misleads the update directions).

A standard alternative to Newton's method is a class of quasi-Newton methods, which have been widely used in solving convex deterministic optimization:

$$\theta_{t+1} = \theta_t - \eta_t B_t^{-1} g_t \quad (4)$$

where η_t is the stepsize (a.k.a learning rate), B_t is an approximation to the Hessian matrix $\nabla^2 f(\theta_t)$ at θ_t , which is updated based on the well-known secant equation:

$$\begin{aligned} B_{t+1} &= \underset{B}{\operatorname{argmin}} \|B - B_t\| \\ \text{s.t. } B_{t+1} s_t &= y_t \quad (\text{secant equation}) \end{aligned} \quad (5)$$

where $s_t = \theta_{t+1} - \theta_t$ and $y_t = g_{t+1} - g_t$. B_{t+1} is, in the sense of some matrix norm, the closest to B_t among all symmetric matrices that satisfy the secant equation. Each choice of the matrix norm results in a different update formula, such as DFP (Davidon, 1991; Fletcher, 1987) and BFGS (Broyden, 1970; Fletcher, 1970; Goldfarb, 1970; Shanno, 1970). The popularity of this method is due to the fact that only the gradient of the objective function is required at each iteration. Since no second derivatives (Hessian) are required, quasi-Newton method is sometimes more efficient than Newton's method, especially when the computation of Hessian is expensive. To further reduce memory cost, one seminal work is the limited memory BFGS (L-BFGS) (Liu and Nocedal, 1989; Byrd et al., 1995) that achieves desirable linear computational and memory complexity by approximating the Hessian as a series of sum of first order information from previous iterations.

2.3 Problems of quasi-Newton Methods

Despite their impressive successes on convex deterministic optimization, quasi-Newton methods suffer from their own problems in more challenging scenarios. In this section, we mainly discuss three problems preventing quasi-Newton methods from being applied to the scenario of large-scale nonconvex stochastic optimization. Due to these problems, no quasi-Newton methods (to our best knowledge) designed for nonconvex optimization consistently outperform adaptive first-order algorithms w.r.t convergence speed and generalization performance. The main goal of this work is to algorithmically design and experimentally demonstrate a novel quasi-Newton method, in hope of improving the convergence speed and generalization performance of nonconvex stochastic optimization eventually.

Stochastic Variance. One challenge of quasi-Newton methods on nonconvex stochastic optimization (1) is the variance introduced by the stochastic nature of the problem. At each iteration, only the stochastic gradient g_t is available, which is an unbiased estimation of the gradient $\nabla f(\theta_t)$ and may lead to an erroneous approximation of Hessian (Byrd et al., 2011).

Nonconvexity. Another key challenge in designing such quasi-Newton methods lies in the difficulty of preserving the positive-definiteness of B_t in (5), due to the nonconvexity of the objective function. What is worse is that performing line search is infeasible in the stochastic setting, due to the presence of noise in the stochastic gradients (Wang et al., 2017).

Computational and Memory Efficiency. Even though quasi-Newton methods are more efficient than Newton’s method, the time and memory complexities are still relatively large compared with adaptive first-order methods. For instance, L-BFGS requires to store first-order information from m previous iterations with commonly $m \geq 5$, which is still too expensive for deep neural networks containing millions of parameters. Moreover, adapting quasi-Newton methods to nonconvex stochastic optimization probably introduces additional computation, further slowing down these methods.

3. Adaptive Parameter-Wise Diagonal Quasi-Newton

With the end goal of designing an efficient quasi-Newton method to solve the problem in (1) in mind, we first propose to approximate the Hessian with a diagonal matrix, whose elements are determined by the variational approach subject to the *parameter-wise* weak secant equation (§3.1). Then, we explain our stepsize bias correction technique to reduce the stochastic variance in §3.2. To handle nonconvexity, we directly use the rectified absolute value of the diagonally approximated Hessian as the preconditioning of the gradient (§3.3). The initialization technique of APOLLO allows us to eliminate one hyper-parameter (§3.4). At last, we provide a theoretical analysis of APOLLO’s convergence in both convex optimization and nonconvex stochastic optimization (§3.5). The pseudo-code is shown in Algorithm 1.

3.1 Quasi-Newton Methods with Diagonal Hessian Approximation

As discussed in Bordes et al. (2009), designing an efficient stochastic quasi-Newton algorithm involves a careful trade-off between the sparsity of the approximation matrix B_t and the quality of its approximation of the Hessian H_t , and diagonal approximation is a reasonable choice (Becker et al., 1988; Zhu et al., 1999). If B is chosen to be a diagonal matrix satisfying (5), one can obtain a formula similar to the SGD-QN algorithm (Bordes et al., 2009).

An alternative of the secant equation in the updating formula (5), as first introduced by Nazareth (1995), is the weak secant equation (Dennis and Wolkowicz, 1993):

$$\begin{aligned} B_{t+1} &= \underset{B}{\operatorname{argmin}} \|B - B_t\| \\ \text{s.t. } s_t^T B_{t+1} s_t &= s_t^T y_t \quad (\text{weak secant equation}) \end{aligned} \quad (6)$$

The motivation of using the weak secant condition in diagonal quasi-Newton method is straight-forward: the standard mean-value theorem might not necessarily hold for vector-valued functions expressed in the secant equation, $B_{t+1} s_t = y_t \approx \nabla^2 f(\theta_t) s_t$. Thus, we do not know whether there exists a vector $\tilde{\theta} \in \mathcal{R}^d$ such that $y_t = \nabla^2 f(\tilde{\theta}) s_t$ (Dennis and Moré, 1977). On the other hand, the Taylor theorem ensures that there exists such $\tilde{\theta}$ that $s_t^T y_t = s_t^T \nabla^2 f(\tilde{\theta}) s_t$, leading to the reasonable assumption of the weak secant condition (6).

Based on the variational technique proposed in Zhu et al. (1999), the solution of (6) with Frobenius norm is:

$$\Lambda \triangleq B_{t+1} - B_t = \frac{s_t^T y_t - s_t^T B_t s_t}{\|s_t\|_4^4} \operatorname{Diag}(s_t^2) \quad (7)$$

where s_t^2 is the element-wise square vector of s_t , $\operatorname{Diag}(s_t^2)$ is the diagonal matrix with diagonal elements from vector s_t^2 , and $\|\cdot\|_4$ is the 4-norm of a vector.

Parameter-Wise Weak Secant Condition. However, in optimization problems with high-dimensional parameter space, such as training deep neural networks with millions of parameters, the weak secant condition might be too flexible to produce a good Hessian approximation. In the setting of decoupled parameters (§2.1), we propose a parameter-wise version of the weak secant equation to achieve a trade-off between the secant and weak secant conditions: for each parameter $\theta^{(l)} \in \theta$, we update B corresponding to $\theta^{(l)}$ by solving (6) individually. Remarkably, the secant condition restricts B with an equation of a d -dimensional vector, while the weak secant condition relaxes it with a 1-dimensional scalar. The parameter-wise weak secant condition expresses the restriction as a l -dimension vector ($1 < l < d$), resulting in a reasonable trade-off. The updating formula is the same as (7) for each parameter-wise B .

3.2 Stepsize Bias Correction

To mitigate the stochastic variance problem in stochastic quasi-Newton methods, APOLLO utilizes stepsize bias correction on the stochastic gradients at each step t . We know that the optimal stepsize η_t equals to 1 w.r.t the *quadratic approximation* underlining Newton's method, if the Hessian approximation B_t and the stochastic gradient g_t are close to the exact Hessian H_t and gradient $\nabla f(\theta_t)$, respectively. Inspired by this, we correct the stepsize bias in the stochastic gradient g_t by replacing it with a corrected gradient $g'_t = \eta_t g_t$. Together with the corresponding corrected $y'_t = g'_{t+1} - g'_t = \eta_t y_t$, we correct the updating term Λ of B_t in (7) by replacing y_t with y'_t :

$$\Lambda' = \frac{s_t^T y'_t - s_t^T B_t s_t}{\|s_t\|_4^4} \operatorname{Diag}(s_t^2) = -\frac{d_t^T y_t + d_t^T B_t d_t}{\|d_t\|_4^4} \operatorname{Diag}(d_t^2) \quad (8)$$

where $d_t = -s_t/\eta_t = B_t^{-1} g_t$ is the corrected update direction. Note that after applying the step bias correction, the update formula of B_t in (8) is independent with the stepsize η_t ,

Algorithm 1: APOLLO, our proposed algorithm for nonconvex stochastic optimization. All operations on vector are element-wise. Good default settings are $\beta = 0.9$ and $\epsilon = 1e^{-4}$.

```

Initial:  $m_0, d_0, B_0 \leftarrow 0, 0, 0$  // Initialize  $m_0, d_0, B_0$  to zero
while  $t \in \{0, \dots, T\}$  do
  for  $\theta \in \{\theta^1, \dots, \theta^L\}$  do
     $g_{t+1} \leftarrow \nabla f_t(\theta_t)$  // Calculate gradient at step  $t$ 
     $m_{t+1} \leftarrow \frac{\beta(1-\beta^t)}{1-\beta^{t+1}}m_t + \frac{1-\beta}{1-\beta^{t+1}}g_{t+1}$  // Update bias-corrected moving
     $\alpha \leftarrow \frac{d_t^T(m_{t+1}-m_t)+d_t^T B_t d_t}{(\|d_t\|_4+\epsilon)^4}$  // Calculate coefficient of  $B$  update
     $B_{t+1} \leftarrow B_t - \alpha \cdot \text{Diag}(d_t^2)$  // Update diagonal Hessian
     $D_{t+1} \leftarrow \text{rectify}(B_{t+1}, 1)$  // Handle nonconvexity
     $d_{t+1} \leftarrow D_{t+1}^{-1}m_{t+1}$  // Calculate update direction
     $\theta_{t+1} \leftarrow \theta_t - \eta_{t+1}d_{t+1}$  // Update parameters
  end
end
return  $\theta_T$ 

```

eliminating the stepsize bias. Technically, the stepsize bias correction is designed to reduce the stochastic variance, rather than entirely discarding the stepsize. The APOLLO algorithm (Algorithm 1) still incorporates the stepsize at every iteration to enforce convergence.

Based on previous studies, incorporating exponential moving averages (EMVs) for the stochastic gradients significantly reduces the variance (Kingma and Ba, 2015). We follow these work and apply EMV to g_t , together with the initialization bias correction:

$$m_{t+1} = \frac{\beta(1-\beta^t)}{1-\beta^{t+1}}m_t + \frac{1-\beta}{1-\beta^{t+1}}g_{t+1} \quad (9)$$

where $0 < \beta < 1$ is the decay rate of EMV and y_t in (8) is written as $m_{t+1} - m_t$. Note that we do not apply moving average methods to the approximated Hessian, though the diagonal matrix is easier to be explicitly formed to average than full matrices. Investigating the moving average of the diagonal B_t might be an interesting direction of future work.

3.3 Rectified Absolute Value of Hessian for Nonconvexity

To guarantee convergence, quasi-Newton methods require the approximated Hessian matrix B_t to be positive definite at each step. The common strategy in previous studies is to solve the updating formula in (5) by restricting the candidate matrix B to be symmetric positive definite. It is known that the BFGS update preserves the positive-definiteness of B_{t+1} as long as the curvature condition $s_t^T y_t > 0$ holds, which can be guaranteed for strongly convex problem. For nonconvex problem, the curvature condition can be satisfied by performing a line search, which is, however, expensive or even infeasible in stochastic setting, because the exact function values and gradient information are unavailable. Wang et al. (2017) proposed the stochastic damped L-BFGS (SdLBFGS) method that implicitly generates a positive definite matrix without line search. However, it usually requires large history size ($m \geq 100$) to guarantee convergence, which is infeasible for large-scale optimization.

To handle nonconvexity, we adopt a different strategy that does not require the solution of B_t in (5) to be positive definite. Intuitively, we search for B_t that is a good approximation of the real Hessian, which is not necessarily positive definite in nonconvex problem. When we use B_t as preconditioning to calculate the update direction, we use its absolute value:

$$|B_t| = \sqrt{B_t^T B_t} \quad (10)$$

where $\sqrt{\cdot}$ is the positive definite square root of a matrix. The motivation of absolute value is straight-forward: for dimensions with large absolute values of curvature, the objective function could be very sharp and we would prefer to take relatively smaller steps than those flatter dimensions. Since APOLLO formulate B_t as a diagonal matrix, the cost of computing $|B_t|$ is marginal.

Rectified Absolute Value of B_t For nonconvex objective functions, there exist inflection points whose curvatures are zero. To prevent the steps from becoming arbitrarily large, we rectify the absolute value of B_t with a convexity hyper-parameter σ :

$$D_t = \text{rectify}(B_t, \sigma) = \max(|B_t|, \sigma) \quad (11)$$

where the $\text{rectify}(\cdot, \sigma)$ function is similar to the rectified linear unit (ReLU) (Nair and Hinton, 2010) with threshold set to σ . The update direction in (8) is then $d_t = D_t^{-1} m_t$.

AdaHessian (Yao et al., 2020) used an idea similar to the absolute values of B_t to handle nonconvexity, where the root mean square averaging is applied to compute the Hessian diagonal. Different from APOLLO, AdaHessian requires second-order information to compute the Hessian matvec oracle and approximate the Hessian diagonal using Hutchinson's method, which is significantly more costly.

3.4 Initialization

The rectified D_t in (11) introduces one more hyper-parameter σ , limiting the application of APOLLO in practice. In this section, we show that the zero initialization approach in APOLLO, which initializes the moving average of gradient m_0 , the parameter update direction d_0 and the diagonal approximation of Hessian B_0 as (vector of) zeros, leads to coupled stepsize η and convexity σ , allowing us to eliminate one hyper-parameter of η or σ .

Coupled Stepsize η and Convexity σ . With the zero initialization of m_0 , d_0 and B_0 , the following theorem illustrates the relation between η and σ (details in Appendix A):

Theorem 1 *Given zero initialization of m_0 , d_0 , and B_0 and a fixed parameter initialization θ_0 . Suppose that we have two sets of hyper-parameters η, σ and η', σ' with the same ratio: $\frac{\eta}{\sigma} = \frac{\eta'}{\sigma'}$. Then the convergence trajectories of these two sets of hyper-parameters are exactly the same:*

$$\theta_t = \theta'_t, \quad \forall t \in \{1, \dots, T\}. \quad (12)$$

where θ_t and θ'_t are the parameters of (η, σ) and (η', σ') at iteration t , respectively.

From Theorem 1, we observe that η and σ are coupled with each other and in practice we only need to tune one of them, leaving the other fixed. Therefore, in our experiments (§4), we fix $\sigma = 1$ and tune η on different problems.

Learning Rate Warmup for APOLLO As discussed in Kingma and Ba (2015), zero initialization leads to estimations biased towards zero in the initial iterations. For the moving average m_t , this bias can be corrected by dividing the bias-correction term (9). For d_t and B_t , however, we cannot derive such bias correction terms. Fortunately, a simple linear warmup heuristic of η at the beginning iterations achieves remarkably stable training.

3.5 Convergence Analysis

Similar to previous work (Reddi et al., 2018; Chen et al., 2019; Zhuang et al., 2020), we omit the initialization bias correction step, i.e. we use $m_t = \beta_t m_{t-1} + (1 - \beta_t)g_t$, $0 < \beta_t < 1$, $\forall t \in [T]$.

We first analyze the convergence of APOLLO in convex optimization using the online learning framework (Zinkevich, 2003) for a sequence of convex cost functions $f_1(\theta), f_2(\theta), \dots, f_T(\theta)$.

Theorem 2 (*Convergence in convex optimization*) *Let $\{\theta_t\}$ be the sequence from APOLLO. Suppose $\eta_t = \frac{\eta}{\sqrt{t}}$, $0 < \beta_t \leq \beta \leq 1$, $\|g_t\|_2 \leq G$, $\frac{\|D_{t-1}\|_1}{\eta_{t-1}} \leq \frac{\|D_t\|_1}{\eta_t}$, $\|\theta_t - \theta_{t'}\|_2 \leq D$, $\forall t, t' \in [T]$. For θ_t generated with the APOLLO algorithm, we have the following bound on the regret:*

$$R_T \leq \frac{\sqrt{T}D^2\|D_T\|_1}{2\eta(1-\beta)} + \frac{\eta G^2}{1-\beta}(2\sqrt{T}-1) + \frac{D^2}{2(1-\beta)} \sum_{t=1}^T \frac{\beta_t^2}{\eta_t} \quad (13)$$

The following result falls as an immediate corollary of the above result.

Corollary 2.1 *Suppose $\beta_t = \beta\lambda^{t-1}$, $0 < \lambda < 1$ in Theorem 2, we have*

$$R_T \leq \frac{\sqrt{T}D^2\|D_T\|_1}{2\eta(1-\beta)} + \frac{\eta G^2}{1-\beta}(2\sqrt{T}-1) + \frac{D^2\beta^2}{2\eta(1-\beta)(1-\lambda^2)^2} \quad (14)$$

Theorem 2 implies the regret of APOLLO is upper bounded by $O(\sqrt{T})$ (proof in Appendix B.1). The conditions for Corollary 2.1, as in Reddi et al. (2018), can be relaxed to $\beta_t = \beta/t$ and still ensures a regret of $O(\sqrt{T})$.

For nonconvex case, we analyze the convergence rate of APOLLO with the similar derivations of that in Chen et al. (2019), since APOLLO belongs to the family of *generalized Adam-type* methods (proof in Appendix B.2):

Theorem 3 (*Convergence in nonconvex stochastic optimization*) *Under the assumptions:*

- f is lower bounded and differentiable; $\|\nabla f(\theta) - \nabla f(\theta')\|_2 \leq L\|\theta - \theta'\|_2$, $\|D_t\|_\infty < L$, $\forall t, \theta, \theta'$.
- Both the true and stochastic gradient are bounded, i.e. $\|\nabla f(\theta_t)\|_2 \leq H$, $\|g_t\|_2 \leq H$, $\forall t$.
- Unbiased and independent noise in g_t , i.e. $g_t = \nabla f(\theta_t) + \zeta_t$, $\mathbb{E}[\zeta_t] = 0$, and $\zeta_i \perp \zeta_j$, $\forall i \neq j$.

Assume $\eta_t = \frac{\eta}{\sqrt{t}}$, $\beta_t \leq \beta \leq 1$ in non-increasing, $\frac{D_{t-1,j}}{\eta_{t-1}} \leq \frac{D_{t,j}}{\eta_t}$, $\forall t \in [T], j \in [d]$, then:

$$\min_{t \in [T]} \mathbb{E} [\|\nabla f(\theta_t)\|_2^2] \leq \frac{L}{\sqrt{T}}(C_1\eta^2 H^2(1 + \log T) + C_2d\eta + C_3d\eta^2 + C_4) \quad (15)$$

where C_1, C_2, C_3 are constants independent of d and T , C_4 is a constant independent of T , the expectation is taken w.r.t all the randomness corresponding to $\{g_t\}$. Theorem 3 implies the convergence rate for APOLLO in the non-convex case is $O(\log T/\sqrt{T})$, which is similar to Adam-type optimizer (Reddi et al., 2018; Chen et al., 2019). In addition, unlike Theorem 3.1 in Chen et al. (2019), Theorem 3 does not specify the bound of each update $\|\eta_t m_t / D_t\|_2$. This is because that, with conditions $\eta_t \leq \eta$, $\|g_t\|_2 \leq H$ and $D_t \geq 1$, it is straight-forward to derive the bound of $\|\eta_t m_t / D_t\|_2 \leq \eta H = G$.

4. Experiments

To evaluate APOLLO, we conduct experiments on four benchmark datasets across three tasks of CV and NLP that are commonly used to evaluate optimization algorithms: CIFAR-10 (Krizhevsky and Hinton, 2009) and ImageNet (Deng et al., 2009) for image classification; One Billion Words (Chelba et al., 2013) for language modeling; and WMT 2014 English-German for neural machine translation. The five baseline methods we compare with are SGD with momentum (Bottou and Bousquet, 2008), Adam (Kingma and Ba, 2015), Rectified Adam (RAdam) (Liu et al., 2020), AdaBelief (Zhuang et al., 2020), and AdaHessian (Yao et al., 2020). Following Loshchilov and Hutter (2019), we decouple weight decays in Adam, RAdam, AdaBelief and AdaHessian in all the experiments¹. For each experiment, we report the average over 5 runs. More detailed descriptions, results and analysis of the conducted experiments are provided in Appendix D.

4.1 Image Classification

We begin our experiments with an evaluation of the convergence and generalization performance on image classification. We use ResNet-110² for CIFAR-10 and standard ResNext-50 (Xie et al., 2017) for ImageNet, respectively. The results on CIFAR-10 and ImageNet are presented in Figure 1 and Table 1, together with the five baselines. For each optimizer, we use two scheduling strategies of learning rate decay: i) milestone that decays the learning rate at the end of some predefined epochs; and ii) cosine annealing schedule proposed in Loshchilov and Hutter (2017). All the optimization methods are comprehensively tuned, especially for the learning rate and the rate of weight decay. It is because that the strength of weight decay regularization is co-related with the learning rate, even though the decoupled weight decay technique (Loshchilov and Hutter, 2019) has been applied. The tuning information and the model details are provided in the Appendix D.1.

From Figure 1 and Table 1, we see that APOLLO outperforms the four first-order methods (SGD, Adam, RAdam and AdaBelief) on both the convergence speed and classification accuracy, demonstrating its effectiveness on training the ResNet architectures based on convolutional neural networks (CNNs) (LeCun et al., 1989). Comparing with AdaHessian, APOLLO obtains better test accuracy with similar convergence speed. Note that AdaHessian requires second-order information and is significantly more costly (detailed comparison of time and memory costs in Appendix E.3). Thus, we omit AdaHessian from the following experiments in the rest of this paper.

Table 1: Test Acc. on CIFAR-10 and ImageNet.

Method	CIFAR-10		ImageNet	
	milestone	cosine	milestone	cosine
SGD	93.94	94.53	77.57	78.26
Adam	93.74	94.24	76.86	77.54
RAdam	93.88	94.38	76.91	77.68
AdaBelief	94.03	94.51	77.55	78.22
AdaHessian	93.97	94.48	–	–
APOLLO	94.21	94.64	77.85	78.45

1. For AdaBelief, we also tried standard L_2 regularization. But the accuracies are consistently worse than the models with decoupled weight decay.
2. ResNet-110 is a modified (small) version of ResNet-18 to adapt the image size 32×32 in CIFAR-10.

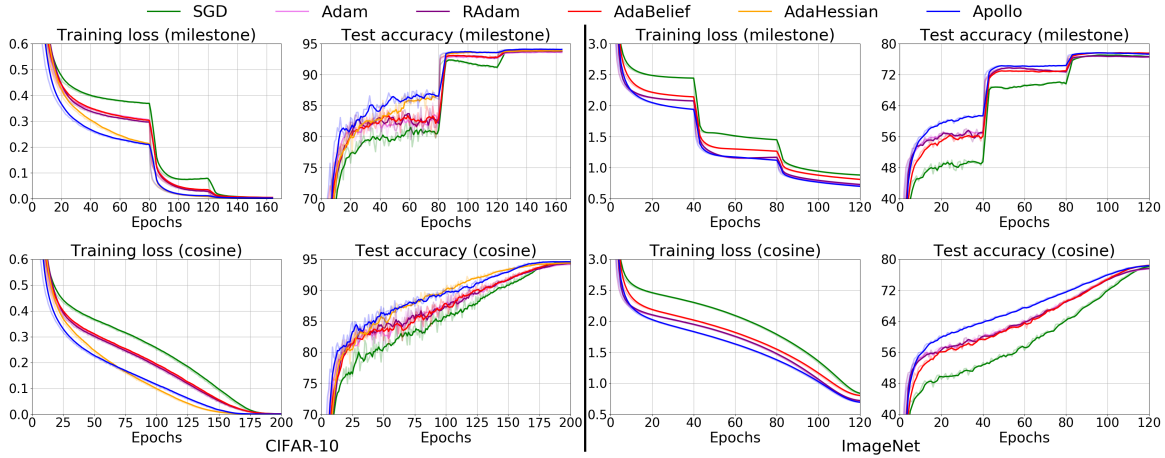


Figure 1: Training loss and test accuracy of ResNet-110 on CIFAR-10 and ResNeXt-50 on ImageNet, with two schedule strategies of learning rate decay.

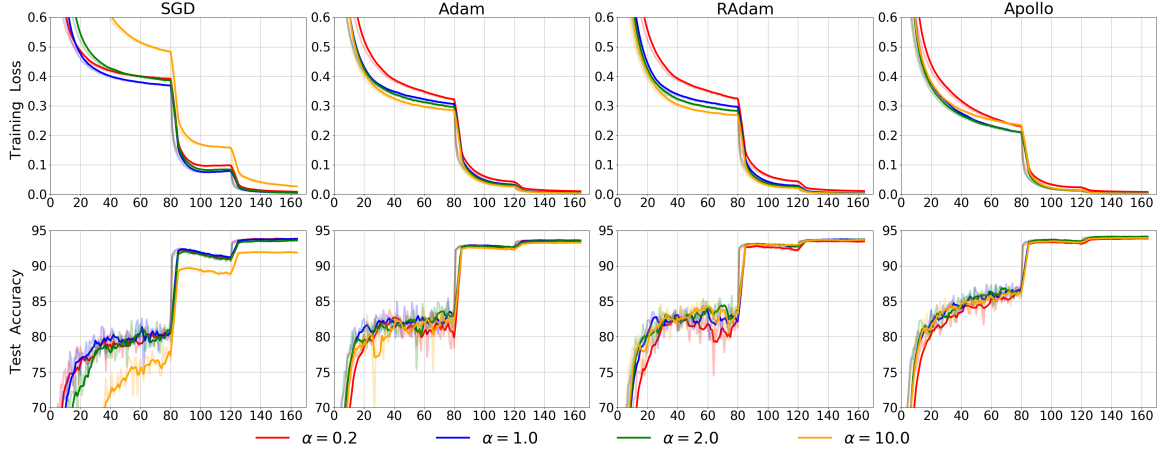


Figure 2: SGD, Adam, RAdam and APOLLO with different learning rates on CIFAR-10.

Robustness to Learning Rate Change. Besides performance improvements, we also investigate the robustness of different optimization methods to the change of learning rate. For each optimizer, we use the learning rate in the previous experiment (Table 1) as the base, i.e. 0.1 for SGD, 0.001 for Adam and RAdam, and 1.0 for APOLLO. Then, we explore different learning rates that are α times of the base learning rate, with $\alpha \in \{0.2, 1.0, 2.0, 10.0\}$. As mentioned above, we observed that the strength of weight decay regularization is co-related with the learning rate, even for Adam and RAdam with decoupled weight decay (Loshchilov and Hutter, 2019). To eliminate the impact of weight decay, we adjust the weight decay rates according to the factor α . Experimental results with ResNet-110 on CIFAR-10 are summarized in Figure 2. After correcting the impact of weight decay, all the optimization methods, except SGD with $\alpha = 10.0$, achieves consistent model performance (highly overlapped training and test curves with each other), while APOLLO slightly improves the robustness of model training over the three baseline methods. More detailed analysis on the effect of weight decay is provided in Appendix E.2.

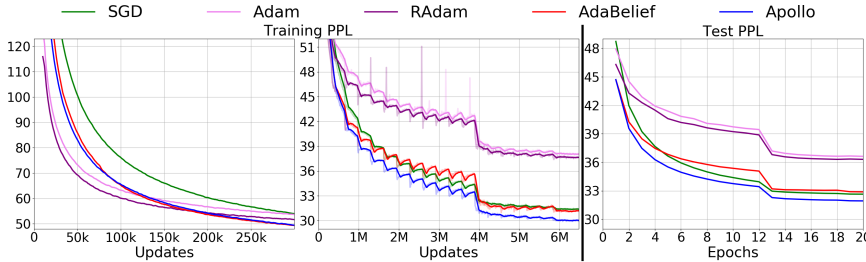


Figure 3: Language modeling (LSTMs) on One Billion Words.

Method	PPL
SGD	32.65
Adam	36.68
RAdam	36.20
AdaBelief	32.83
APOLLO	31.94

Table 2: Test PPL.

4.2 Language Modeling

To evaluate APOLLO on Recurrent Neural Networks (RNNs) that are applied in a wide range of NLP tasks (Graves, 2013), we conduct experiments on the One Billion Words dataset (Chelba et al., 2013), using a two-layer LSTM network for language modeling (details in Appendix D.2).

Figure 3 and Table 2 illustrate the perplexity (PPL) of training and test for APOLLO and four baseline methods, including SGD, Adam, RAdam and AdaBelief. As shown in Figure 3, although APOLLO is slower than Adam-type methods in the first few updates, its convergence is much faster after that. On generalization performance, APOLLO achieves significant improvements (more than 4.0 PPL points on test data) over Adam and RAdam. In addition, APOLLO also outperforms AdaBelief, which obtains the lowest PPL among the three Adam-type optimization methods³. This demonstrates the effectiveness of APOLLO on training LSTM-based neural architectures.

Training Stability. From the middle plot Figure 3 we see that the training losses of Adam and RAdam may suddenly increase. This occurred in all the runs of experiments using Adam and RAdam, and we selected these successfully converged — the loss went back to normal after some updates, and discarded those failed to converge — the model crashed due to loss numerical overflow. The models optimized with APOLLO never suffered from this issue, demonstrating the convergence stability of it.

4.3 Neural Machine Translation

To evaluate APOLLO on Attention-based Transformer architecture (Vaswani et al., 2017), we train the Transformer-base model on the WMT2014 English-German (EN-DE) dataset (around 4.5M sentence pairs). We use the same data preprocessing steps as in Ma et al. (2019) (details in Appendix D.3). We compare APOLLO with the same four baseline methods in the experiments of language modeling. For each experiment, we report the mean and standard variance over 5 runs. From Table 3, the first interesting observation is that SGD performs much worse than Adam-type

Table 3: Test BLEU.

Method	BLEU
SGD	26.59 \pm 0.07
Adam	27.84 \pm 0.12
RAdam	28.15 \pm 0.15
AdaBelief	28.14 \pm 0.11
APOLLO	28.34\pm0.10

3. We found that AdaBelief is very sensitive to the value of ϵ . The result in Table 2 is obtained using $\epsilon = 1e^{-12}$. With other values, e.g. $1e^{-8}$ or $1e^{-16}$, the PPL points of AdaBelief are even higher than Adam and RAdam. See Appendix D.2 for the details of hyper-parameter tuning.

methods (which is opposite to its behaviour for ResNet- and LSTM-based neural architectures). Similar observations about SGD were reported in (Yao et al., 2020; Zhang et al., 2020). Despite this, APOLLO obtains improvements over all the baseline methods for NMT with transformers.

5. Related Work

Stochastic Quasi-Newton Methods. In the literature of (nonconvex) stochastic quasi-Newton methods, several algorithms have been developed recently for large-scale machine learning problems: oLBFGS (Schraudolph et al., 2007; Mokhtari and Ribeiro, 2015), RES (Mokhtari and Ribeiro, 2014), SFO (Sohl-Dickstein et al., 2014), SQN (Byrd et al., 2016), SdLBFGS (Wang et al., 2017), and AdaQN (Keskar and Berahas, 2016), among which only SdLBFGS and AdaQN are designed to solve nonconvex optimization problems. The SdLBFGS algorithm carefully controls the quality of modified BFGS updates to preserve the positive-definiteness of B_t in (5) without line search. AdaQN shares a similar idea but is specifically designed for RNNs by refining the initial L-BFGS scaling, step acceptance control and choice of curvature information matrix, and adopting the SQN framework (Byrd et al., 2016). Different from these two methods, APOLLO does not require B_t in (5) to be positive definite, but replacing it with its rectified absolute value to handle nonconvexity. Moreover, both SdLBFGS and AdaQN use the updating formula similar to L-BFGS and require even larger history size (commonly ≥ 100) to guarantee convergence, preventing them from being applied to large-scale optimization. For comprehensive comparison of SdLBFGS with Apollo, we conducted experiments with small toy CNN models (details in Appendix F).

Adaptive First-Order Methods. From the diagonal approximation of Hessian, APOLLO is also related to those diagonally-scaled first-order algorithms, such as AdaGrad (Duchi et al., 2011), RMSProp (Tieleman and Hinton, 2012), AdaDelta (Zeiler, 2012), and Adam (Kingma and Ba, 2015). Subsequently, a number of techniques have emerged to theoretically justify and algorithmically improve Adam, including AMSGrad (Reddi et al., 2018), AdaBound (Luo et al., 2019), RAdam (Liu et al., 2020) and AdaBelief (Zhuang et al., 2020). The main difference is that the diagonal preconditioning in APOLLO is directly derived from the quasi-Newton updating formula (6). In terms of memory efficiency, Anil et al. (2019) and Chen et al. (2020) further reduces the memory cost of adaptive methods, and Agarwal et al. (2019) proposed an efficient method for full-matrix adaptive regularization.

Stochastic Second-Order Hessian-Free Methods. Stochastic Second-Order Hessian-Free methods (Martens, 2010; Martens and Sutskever, 2011) implicitly solve quadratic models using matrix-vector products. Dauphin et al. (2014) argued the existence of saddle points and proposed a method to rapidly escape them. K-FAC (Martens and Grosse, 2015) computes a second-order step by constructing an invertible approximation of the Fisher information matrix in an online fashion. Shampoo (Gupta et al., 2018) approximates the Fisher information matrix using low-rank decomposition. Recently, Yao et al. (2020) proposed AdaHessian, which approximates the Hessian diagonal using Hutchinson’s method. These second-order methods differ from APOLLO mainly in the request of second-order information of the objective function at each iteration.

6. Conclusion and Extensions

We have introduced APOLLO, a simple and computationally efficient quasi-Newton algorithm for nonconvex stochastic optimization. This method is aimed towards large-scale optimization problems in the sense of large datasets and/or high-dimensional parameter spaces such as machine learning with deep neural networks. Experimental results on three CV and NLP tasks demonstrate the effectiveness of APOLLO, in terms of both convergence speed and generalization performance. We briefly outline a few extensions to APOLLO that we want to explore in future work.

Parameter-Wise Gradient Clipping. The standard gradient clipping method (Pascanu et al., 2013) is to clip the gradients based on the norm computed over gradients of all the parameters together. A modification of gradient clipping to properly apply it to APOLLO is to clip the gradient of each parameter individually based on its own norm. Preliminary results are provided in Appendix E.4.

Decoupled Weight Decay in APOLLO. (Loshchilov and Hutter, 2019) demonstrated that L_2 regularization is not identical to weight decay for adaptive gradient methods and proposed Adam with decoupled weight decay (AdamW). The application of decoupled weight decay to APOLLO is slightly different from AdamW as APOLLO memorizes the update direction of the last iteration d_t to update the diagonal Hessian. The algorithm of APOLLO with decoupled weight decay is in Appendix C.

Making APOLLO Scale-Invariant. An important advantage of adaptive optimization methods, including Adam and its variants, is that they are inherently scale-invariant — invariant with the scale of the objective function. The property of scale-invariance yields more consistent hyper-parameters of these adaptive methods than SGD across different machine learning tasks. Unfortunately, APOLLO does not hold the property of scale-invariance, and we need to ask if it is possible to make APOLLO scale-invariant. Interestingly, it is quite easy to develop a scale-invariant version of APOLLO by applying a simple modification. We provide more details about scale-invariant APOLLO in Appendix G.

References

Naman Agarwal, Brian Bullins, Xinyi Chen, Elad Hazan, Karan Singh, Cyril Zhang, and Yi Zhang. Efficient full-matrix adaptive regularization. In *International Conference on Machine Learning*, pages 102–110, 2019.

Rohan Anil, Vineet Gupta, Tomer Koren, and Yoram Singer. Memory efficient adaptive optimization. In *Advances in Neural Information Processing Systems*, pages 9749–9758, 2019.

Sue Becker, Yann Le Cun, et al. Improving the convergence of back-propagation learning with second order methods. In *Proceedings of the 1988 connectionist models summer school*, pages 29–37, 1988.

Antoine Bordes, Léon Bottou, and Patrick Gallinari. SGD-QN: Careful quasi-newton stochastic gradient descent. *The Journal of Machine Learning Research*, 10:1737–1754, 2009.

Léon Bottou and Olivier Bousquet. The tradeoffs of large scale learning. In *Advances in neural information processing systems*, pages 161–168, 2008.

Charles G Broyden. Quasi-newton methods and their application to function minimisation. *Mathematics of Computation*, 21(99):368–381, 1967.

Charles George Broyden. The convergence of a class of double-rank minimization algorithms. *IMA Journal of Applied Mathematics*, 6(1):76–90, 1970.

Richard H Byrd, Peihuang Lu, Jorge Nocedal, and Ciyou Zhu. A limited memory algorithm for bound constrained optimization. *SIAM Journal on scientific computing*, 16(5):1190–1208, 1995.

Richard H Byrd, Gillian M Chin, Will Neveitt, and Jorge Nocedal. On the use of stochastic hessian information in optimization methods for machine learning. *SIAM Journal on Optimization*, 21(3):977–995, 2011.

Richard H Byrd, Samantha L Hansen, Jorge Nocedal, and Yoram Singer. A stochastic quasi-newton method for large-scale optimization. *SIAM Journal on Optimization*, 26(2):1008–1031, 2016.

Ciprian Chelba, Tomas Mikolov, Mike Schuster, Qi Ge, Thorsten Brants, Philipp Koehn, and Tony Robinson. One billion word benchmark for measuring progress in statistical language modeling. *arXiv preprint arXiv:1312.3005*, 2013.

X Chen, M Hong, S Liu, and R Sun. On the convergence of a class of adam-type algorithms for non-convex optimization. In *7th International Conference on Learning Representations, ICLR 2019*, 2019.

Xinyi Chen, Naman Agarwal, Elad Hazan, Cyril Zhang, and Yi Zhang. Extreme tensoring for low-memory preconditioning. In *International Conference on Learning Representations*, 2020.

Yann N Dauphin, Razvan Pascanu, Caglar Gulcehre, Kyunghyun Cho, Surya Ganguli, and Yoshua Bengio. Identifying and attacking the saddle point problem in high-dimensional non-convex optimization. In *Advances in neural information processing systems*, pages 2933–2941, 2014.

William C Davidon. Variable metric method for minimization. *SIAM Journal on Optimization*, 1(1):1–17, 1991.

Jia Deng, Wei Dong, Richard Socher, Li-Jia Li, Kai Li, and Li Fei-Fei. Imagenet: A large-scale hierarchical image database. In *2009 IEEE conference on computer vision and pattern recognition*, pages 248–255. Ieee, 2009.

John E Dennis, Jr and Jorge J Moré. Quasi-newton methods, motivation and theory. *SIAM review*, 19(1):46–89, 1977.

John E Dennis, Jr and Henry Wolkowicz. Sizing and least-change secant methods. *SIAM Journal on Numerical Analysis*, 30(5):1291–1314, 1993.

John Duchi, Elad Hazan, and Yoram Singer. Adaptive subgradient methods for online learning and stochastic optimization. *Journal of machine learning research*, 12(7), 2011.

Roger Fletcher. A new approach to variable metric algorithms. *The computer journal*, 13(3), 1970.

Roger Fletcher. *Practical methods of optimization*. John Wiley & Sons, 1987.

D Goldfarb. A family of variable metric updates derived by variational means. *Mathematics of Computation*, 24(109):23–26, 1970.

Alex Graves. Generating sequences with recurrent neural networks. *arXiv preprint:1308.0850*, 2013.

Vineet Gupta, Tomer Koren, and Yoram Singer. Shampoo: Preconditioned stochastic tensor optimization. *arXiv preprint arXiv:1802.09568*, 2018.

Kaiming He, Xiangyu Zhang, Shaoqing Ren, and Jian Sun. Deep residual learning for image recognition. In *Proceedings of the IEEE conference on computer vision and pattern recognition*, pages 770–778, 2016.

Geoffrey Hinton, Li Deng, Dong Yu, George E Dahl, Abdel-rahman Mohamed, Navdeep Jaitly, Andrew Senior, Vincent Vanhoucke, Patrick Nguyen, Tara N Sainath, et al. Deep neural networks for acoustic modeling in speech recognition: The shared views of four research groups. *IEEE Signal processing magazine*, 29(6):82–97, 2012.

Geoffrey E Hinton and Ruslan R Salakhutdinov. Reducing the dimensionality of data with neural networks. *science*, 313(5786):504–507, 2006.

Sepp Hochreiter and Jürgen Schmidhuber. Long short-term memory. *Neural computation*, 9(8):1735–1780, 1997.

Nitish Shirish Keskar and Albert S Berahas. AdaQN: An adaptive quasi-newton algorithm for training rnns. In *Joint European Conference on Machine Learning and Knowledge Discovery in Databases*, pages 1–16. Springer, 2016.

Diederik P Kingma and Jimmy Ba. Adam: A method for stochastic optimization. In *International Conference on Learning Representations*, 2015.

Alex Krizhevsky and Geoffrey Hinton. Learning multiple layers of features from tiny images. Technical report, Citeseer, 2009.

Yann LeCun, Bernhard Boser, John S Denker, Donnie Henderson, Richard E Howard, Wayne Hubbard, and Lawrence D Jackel. Backpropagation applied to handwritten zip code recognition. *Neural computation*, 1(4):541–551, 1989.

Yann LeCun, Léon Bottou, Yoshua Bengio, and Patrick Haffner. Gradient-based learning applied to document recognition. *Proceedings of the IEEE*, 86(11):2278–2324, 1998.

Yingkai Li and Huidong Liu. Implementation of stochastic quasi-newton’s method in pytorch. *arXiv preprint arXiv:1805.02338*, 2018.

Dong C Liu and Jorge Nocedal. On the limited memory bfgs method for large scale optimization. *Mathematical programming*, 45(1-3):503–528, 1989.

Liyuan Liu, Haoming Jiang, Pengcheng He, Weizhu Chen, Xiaodong Liu, Jianfeng Gao, and Jiawei Han. On the variance of the adaptive learning rate and beyond. In *International Conference on Learning Representations*, 2020.

Ilya Loshchilov and Frank Hutter. SGDR: Stochastic gradient descent with warm restarts. In *International Conference on Learning Representations*, 2017.

Ilya Loshchilov and Frank Hutter. Decoupled weight decay regularization. In *International Conference on Learning Representations*, 2019.

Liangchen Luo, Yuanhao Xiong, Yan Liu, and Xu Sun. Adaptive gradient methods with dynamic bound of learning rate. In *International Conference on Learning Representations*, 2019.

Xuezhe Ma and Eduard Hovy. End-to-end sequence labeling via bi-directional LSTM-CNNs-CRF. In *Proceedings of the 54th Annual Meeting of the Association for Computational Linguistics (Volume 1: Long Papers)*, pages 1064–1074, Berlin, Germany, August 2016.

Xuezhe Ma, Chunting Zhou, Xian Li, Graham Neubig, and Eduard Hovy. Flowseq: Non-autoregressive conditional sequence generation with generative flow. In *Proceedings of the 2019 Conference on Empirical Methods in Natural Language Processing*, pages 4282–4292, Hong Kong, November 2019.

James Martens. Deep learning via hessian-free optimization. In *Proceedings of the 27th International Conference on International Conference on Machine Learning*, pages 735–742, 2010.

James Martens and Roger Grosse. Optimizing neural networks with kronecker-factored approximate curvature. In *International conference on machine learning*, pages 2408–2417, 2015.

James Martens and Ilya Sutskever. Learning recurrent neural networks with hessian-free optimization. In *Proceedings of the 28th international conference on machine learning (ICML-11)*, pages 1033–1040. Citeseer, 2011.

Aryan Mokhtari and Alejandro Ribeiro. Res: Regularized stochastic bfgs algorithm. *IEEE Transactions on Signal Processing*, 62(23):6089–6104, 2014.

Aryan Mokhtari and Alejandro Ribeiro. Global convergence of online limited memory bfgs. *The Journal of Machine Learning Research*, 16(1):3151–3181, 2015.

Vinod Nair and Geoffrey E Hinton. Rectified linear units improve restricted boltzmann machines. In *ICML*, 2010.

JL Nazareth. If quasi-newton then why not quasi-cauchy. *SIAG/Opt Views-and-news*, 6: 11–14, 1995.

Jorge Nocedal and Stephen Wright. *Numerical optimization*. Springer Science & Business Media, 2006.

Myle Ott, Sergey Edunov, Alexei Baevski, Angela Fan, Sam Gross, Nathan Ng, David Grangier, and Michael Auli. FairSeq: A fast, extensible toolkit for sequence modeling. In *Proceedings of the 2019 Conference of the North American Chapter of the Association for Computational Linguistics (Demonstrations)*, pages 48–53, 2019.

Razvan Pascanu, Tomas Mikolov, and Yoshua Bengio. On the difficulty of training recurrent neural networks. In *International conference on machine learning*, pages 1310–1318, 2013.

Ning Qian. On the momentum term in gradient descent learning algorithms. *Neural networks*, 12(1):145–151, 1999.

Sashank J Reddi, Satyen Kale, and Sanjiv Kumar. On the convergence of adam and beyond. In *International Conference on Learning Representations*, 2018.

Herbert Robbins and Sutton Monro. A stochastic approximation method. *The annals of mathematical statistics*, pages 400–407, 1951.

Sebastian Ruder. An overview of gradient descent optimization algorithms. *arXiv preprint arXiv:1609.04747*, 2016.

David E Rumelhart, Geoffrey E Hinton, and Ronald J Williams. Learning internal representations by error propagation. Technical report, California Univ San Diego La Jolla Inst for Cognitive Science, 1985.

Nicol N Schraudolph, Jin Yu, and Simon Günter. A stochastic quasi-newton method for online convex optimization. In *Artificial intelligence and statistics*, pages 436–443, 2007.

David F Shanno. Conditioning of quasi-newton methods for function minimization. *Mathematics of computation*, 24(111):647–656, 1970.

Jascha Sohl-Dickstein, Ben Poole, and Surya Ganguli. Fast large-scale optimization by unifying stochastic gradient and quasi-newton methods. In *International Conference on Machine Learning*, pages 604–612, 2014.

Nitish Srivastava, Geoffrey Hinton, Alex Krizhevsky, Ilya Sutskever, and Ruslan Salakhutdinov. Dropout: a simple way to prevent neural networks from overfitting. *The journal of machine learning research*, 15(1):1929–1958, 2014.

Christian Szegedy, Vincent Vanhoucke, Sergey Ioffe, Jon Shlens, and Zbigniew Wojna. Rethinking the inception architecture for computer vision. In *Proceedings of the IEEE conference on computer vision and pattern recognition*, pages 2818–2826, 2016.

Tijmen Tieleman and Geoffrey Hinton. Lecture 6.5-rmsprop: Divide the gradient by a running average of its recent magnitude. *COURSERA: Neural networks for machine learning*, 4(2), 2012.

Ashish Vaswani, Noam Shazeer, Niki Parmar, Jakob Uszkoreit, Llion Jones, Aidan N Gomez, Łukasz Kaiser, and Illia Polosukhin. Attention is all you need. In *Advances in neural information processing systems*, pages 5998–6008, 2017.

Xiao Wang, Shiqian Ma, Donald Goldfarb, and Wei Liu. Stochastic quasi-newton methods for nonconvex stochastic optimization. *SIAM Journal on Optimization*, 27(2):927–956, 2017.

Ashia C Wilson, Rebecca Roelofs, Mitchell Stern, Nati Srebro, and Benjamin Recht. The marginal value of adaptive gradient methods in machine learning. In *Advances in neural information processing systems*, pages 4148–4158, 2017.

Philip Wolfe. The secant method for simultaneous nonlinear equations. *Communications of the ACM*, 2(12):12–13, 1959.

Saining Xie, Ross Girshick, Piotr Dollár, Zhuowen Tu, and Kaiming He. Aggregated residual transformations for deep neural networks. In *Proceedings of the IEEE conference on computer vision and pattern recognition*, pages 1492–1500, 2017.

Zhewei Yao, Amir Gholami, Sheng Shen, Kurt Keutzer, and Michael W Mahoney. ADA-HESSIAN: An adaptive second order optimizer for machine learning. *arXiv preprint arXiv:2006.00719*, 2020.

Wei Yuan and Kai-Xin Gao. EAdam optimizer: How *epsilon* impact adam. *arXiv preprint arXiv:2011.02150*, 2020.

Matthew D Zeiler. Adadelta: an adaptive learning rate method. *arXiv preprint:1212.5701*, 2012.

Jingzhao Zhang, Sai Praneeth Karimireddy, Andreas Veit, Seungyeon Kim, Sashank Reddi, Sanjiv Kumar, and Suvrit Sra. Why are adaptive methods good for attention models? *Advances in Neural Information Processing Systems*, 33, 2020.

Mingfa Zhu, John Lawrence Nazareth, and Henry Wolkowicz. The quasi-cauchy relation and diagonal updating. *SIAM Journal on Optimization*, 9(4):1192–1204, 1999.

Juntang Zhuang, Tommy Tang, Yifan Ding, Sekhar C Tatikonda, Nicha Dvornek, Xenophon Papademetris, and James Duncan. Adabelief optimizer: Adapting stepsizes by the belief in observed gradients. *Advances in Neural Information Processing Systems*, 33, 2020.

Martin Zinkevich. Online convex programming and generalized infinitesimal gradient ascent. In *Proceedings of the 20th international conference on machine learning (icml-03)*, pages 928–936, 2003.

Appendix: Apollo: An Adaptive Parameter-wise Diagonal Quasi-Newton Method for Nonconvex Stochastic Optimization

Appendix A. Coupled Stepsize and Convexity

Before proving Theorem 1, we first define the notations.

Let $\alpha = \frac{\eta'}{\eta} = \frac{\sigma'}{\sigma}$ be the ratio of the two sets of learning rates. Let m'_t , d'_t and B'_t be the corresponding terms of parameter θ'_t at step t for (η', σ') .

Proof of Theorem 1 Proof Induction on the step of updates t , we attempt to prove that at each step t :

$$m_t = m'_t, \quad B'_t = \alpha B_t, \quad \text{and } \theta_t = \theta'_t, \quad \forall t \quad (16)$$

Initial step: when $t = 1$, since $\theta_0 = \theta'_0$, we have $m_1 = m'_1$. With $d_0 = d'_0 = 0$ and (8), we have $B_1 = B'_1 = 0$ and:

$$\begin{aligned} D_1 &= \text{recify}(B_1, \sigma) = \sigma \\ D'_1 &= \text{recify}(B'_1, \sigma') = \sigma' \end{aligned}$$

Then, $D'_1 = \alpha D_1$ and

$$\theta'_1 = \theta'_0 - \eta' D'^{-1}_1 m'_1 = \theta_0 - \eta \alpha (D_1^{-1}/\alpha) m_1 = \theta_0 - \eta D_1^{-1} m_1 = \theta_1.$$

Thus, the statement (16) is true.

Induction on step t : Suppose that the statement (16) is true for all the previous t steps. Now we prove the case $t + 1$. From the inductive assumption and (9), we have,

$$B'_t = \alpha B_t, \quad d'_t = \frac{1}{\alpha} d_t \quad \text{and } m_{t+1} = m'_{t+1}.$$

From (8),

$$\begin{aligned} B'_{t+1} &= B'_t - \frac{d'^T_t y'_t + d'^T_t B'_t d'_t}{\|d'_t\|_4^4} \text{Diag}(d'^2_t) \\ &= \alpha B_t - \frac{(\frac{1}{\alpha} d_t)^T y_t + (\frac{1}{\alpha} d_t)^T (\alpha B_t) (\frac{1}{\alpha} d_t)}{\|(\frac{1}{\alpha} d_t)\|_4^4} \text{Diag}((\frac{1}{\alpha} d_t)^2) \\ &= \alpha B_t - \alpha \frac{d_t^T y_t + d_t^T B_t d_t}{\|d_t\|_4^4} \text{Diag}(d_t^2) \\ &= \alpha B_{t+1}. \end{aligned}$$

Then,

$$\begin{aligned} D'_{t+1} &= \text{recify}(B'_{t+1}, \sigma') \\ &= \text{recify}(\alpha B_{t+1}, \alpha \sigma) \\ &= \alpha \text{recify}(B_{t+1}, \sigma) \\ &= \alpha D_{t+1} \end{aligned}$$

and we have $\theta'_{t+1} = \theta_{t+1}$.

Finally, to sum up with the induction, we have proven Theorem 1. ■

Appendix B. Convergence Analysis

B.1 Convergence Analysis in Convex Optimization

Proof of Theorem 2 Proof Let $\theta^* = \operatorname{argmin}_{\theta \in \mathcal{F}} \sum_{t=1}^T f_t(\theta)$, where \mathcal{F} is the feasible set of θ .

As $\theta_{t+1} - \theta^* = \theta_t - \theta^* - \eta_t D_t^{-1} m_t$ and $m_t = \beta_t m_{t-1} + (1 - \beta_t) g_t$, we have the following:

$$\|D_t^{1/2}(\theta_{t+1} - \theta^*)\|_2^2 \leq \|D_t^{1/2}(\theta_t - \theta^*)\|_2^2 + \|\eta_t D_t^{-1/2} m_t\|_2^2 - 2\eta_t (\beta_t m_{t-1} + (1 - \beta_t) g_t)^T (\theta_t - \theta^*)$$

Then, we have

$$\begin{aligned} g_t^T (\theta_t - \theta^*) &\leq \frac{1}{2\eta_t(1 - \beta_t)} \left[\|D_t^{1/2}(\theta_t - \theta^*)\|_2^2 - \|D_t^{1/2}(\theta_{t+1} - \theta^*)\|_2^2 \right] \\ &\quad + \frac{\eta_t}{2(1 - \beta_t)} \|D_t^{-1/2} m_t\|_2^2 - \frac{\beta_t}{1 - \beta_t} m_{t-1}^T (\theta_t - \theta^*) \\ &\leq \frac{1}{2\eta_t(1 - \beta_t)} \left[\|D_t^{1/2}(\theta_t - \theta^*)\|_2^2 - \|D_t^{1/2}(\theta_{t+1} - \theta^*)\|_2^2 \right] \\ &\quad + \frac{\eta_t}{2(1 - \beta_t)} \|D_t^{-1/2} m_t\|_2^2 + \frac{\eta_t}{2(1 - \beta_t)} \|m_{t-1}\|_2^2 + \frac{\beta_t^2}{2\eta_t(1 - \beta_t)} \|\theta_t - \theta^*\|_2^2 \end{aligned}$$

Using the standard approach of bounding the regret at each step with convexity of the functions $\{f_t\}_{t=1}^T$, we have the following bound of $R_T = \sum_{t=1}^T f_t(\theta_t) - f_t(\theta^*)$:

$$\begin{aligned} \sum_{t=1}^T f_t(\theta_t) - f_t(\theta^*) &\leq \sum_{t=1}^T g_t^T (\theta_t - \theta^*) \\ &\leq \sum_{t=1}^T \frac{1}{2\eta_t(1 - \beta_t)} \left[\|D_t^{1/2}(\theta_t - \theta^*)\|_2^2 - \|D_t^{1/2}(\theta_{t+1} - \theta^*)\|_2^2 \right] \\ &\quad + \sum_{t=1}^T \frac{\eta_t}{2(1 - \beta_t)} \|D_t^{-1/2} m_t\|_2^2 + \frac{\eta_t}{2(1 - \beta_t)} \|m_{t-1}\|_2^2 \\ &\quad + \sum_{t=1}^T \frac{\beta_t^2}{2\eta_t(1 - \beta_t)} \|\theta_t - \theta^*\|_2^2 \end{aligned} \tag{17}$$

As $\|\theta_t - \theta^*\|_2 \leq D$, $\beta_t < \beta < 1$ and $\|D_t\|_1/\eta_t \geq \|D_{t-1}\|_1/\eta_{t-1}$, we have

$$\begin{aligned} &\sum_{t=1}^T \frac{1}{2\eta_t(1 - \beta_t)} \left[\|D_t^{1/2}(\theta_t - \theta^*)\|_2^2 - \|D_t^{1/2}(\theta_{t+1} - \theta^*)\|_2^2 \right] \\ &= \frac{\|D_1^{1/2}(\theta_1 - \theta^*)\|_2^2}{2\eta_1(1 - \beta_1)} + \sum_{t=2}^T \left[\frac{\|D_t^{1/2}(\theta_t - \theta^*)\|_2^2}{2\eta_t(1 - \beta_t)} - \frac{\|D_{t-1}^{1/2}(\theta_t - \theta^*)\|_2^2}{2\eta_{t-1}(1 - \beta_{t-1})} \right] \\ &\leq \frac{\|D_1^{1/2}(\theta_1 - \theta^*)\|_2^2}{2\eta_1(1 - \beta)} + \frac{1}{2(1 - \beta)} \sum_{t=2}^T \left[\frac{\|D_t^{1/2}(\theta_t - \theta^*)\|_2^2}{\eta_t} - \frac{\|D_{t-1}^{1/2}(\theta_t - \theta^*)\|_2^2}{\eta_{t-1}} \right] \\ &\leq \frac{\|(\theta_1 - \theta^*)\|_2^2}{2\eta_1(1 - \beta)} \|D_1^{1/2}\|_2^2 + \frac{1}{2(1 - \beta)} \sum_{t=2}^T \|(\theta_t - \theta^*)\|_2^2 \left[\frac{\|D_t^{1/2}\|_2^2}{\eta_t} - \frac{\|D_{t-1}^{1/2}\|_2^2}{\eta_{t-1}} \right] \end{aligned} \tag{18}$$

Since $\|D_t^{1/2}\|_2^2 = \|D_t\|_1$, we can rewrite the RHS of (18) as:

$$\begin{aligned}
& \frac{\|(\theta_1 - \theta^*)\|_2^2}{2\eta_1(1-\beta)} \|D_1^{1/2}\|_2^2 + \frac{1}{2(1-\beta)} \sum_{t=2}^T \|(\theta_t - \theta^*)\|_2^2 \left[\frac{\|D_t^{1/2}\|_2^2}{\eta_t} - \frac{\|D_{t-1}^{1/2}\|_2^2}{\eta_{t-1}} \right] \\
&= \frac{\|(\theta_1 - \theta^*)\|_2^2}{2\eta_1(1-\beta)} \|D_1\|_1 + \frac{1}{2(1-\beta)} \sum_{t=2}^T \|(\theta_t - \theta^*)\|_2^2 \left[\frac{\|D_t\|_1}{\eta_t} - \frac{\|D_{t-1}\|_1}{\eta_{t-1}} \right] \\
&\leq \frac{D^2}{2\eta_1(1-\beta)} \|D_1\|_1 + \frac{D^2}{2(1-\beta)} \sum_{t=2}^T \left[\frac{\|D_t\|_1}{\eta_t} - \frac{\|D_{t-1}\|_1}{\eta_{t-1}} \right] \\
&= \frac{D^2 \|D_T\|_1}{2\eta_T(1-\beta)} = \frac{\sqrt{T} D^2 \|D_T\|_1}{2\eta(1-\beta)}
\end{aligned} \tag{19}$$

To sum up with (17) and (19), we have

$$\begin{aligned}
R_T &= \sum_{t=1}^T f_t(\theta_t) - f_t(\theta^*) \leq \frac{\sqrt{T} D^2 \|D_T\|_1}{2\eta(1-\beta)} \\
&\quad + \sum_{t=1}^T \frac{\eta_t}{2(1-\beta_t)} \|D_t^{-1/2} m_t\|_2^2 + \frac{\eta_t}{2(1-\beta_t)} \|m_{t-1}\|_2^2 \\
&\quad + \sum_{t=1}^T \frac{\beta_t^2}{2\eta_t(1-\beta_t)} \|\theta_t - \theta^*\|_2^2
\end{aligned} \tag{20}$$

Since the element of D_t is rectified by 1, i.e. $D_{t,i} \geq 1$, and $\|m_t\|_2 \leq G$, $\beta_t < \beta < 1$, we have

$$\begin{aligned}
\sum_{t=1}^T \frac{\eta_t}{2(1-\beta_t)} \|D_t^{-1/2} m_t\|_2^2 + \frac{\eta_t}{2(1-\beta_t)} \|m_{t-1}\|_2^2 &\leq \sum_{t=1}^T \frac{\eta_t}{2(1-\beta_t)} \|m_t\|_2^2 + \frac{\eta_t}{2(1-\beta_t)} \|m_{t-1}\|_2^2 \\
&\leq \frac{G^2}{1-\beta} \sum_{t=1}^T \eta_t = \frac{\eta G^2}{1-\beta} \sum_{t=1}^T \frac{1}{\sqrt{t}} \\
&\leq \frac{\eta G^2}{1-\beta} (2\sqrt{T} - 1)
\end{aligned} \tag{21}$$

The last inequality is due to the following upper bound:

$$\sum_{t=1}^T \frac{1}{\sqrt{t}} \leq \int_{t=1}^T \frac{dt}{\sqrt{t}} = 2\sqrt{T} - 1$$

Again, as $\|\theta_t - \theta^*\|_2 \leq D$ and $\beta_t < \beta < 1$, we have

$$\sum_{t=1}^T \frac{\beta_t^2}{2\eta_t(1-\beta_t)} \|\theta_t - \theta^*\|_2^2 \leq \frac{D^2}{2(1-\beta)} \sum_{t=1}^T \frac{\beta_t^2}{\eta_t} \tag{22}$$

Finally, to sum up with (20), (21) and (22), we have

$$R_T \leq \frac{\sqrt{T}D^2\|D_T\|_1}{2\eta(1-\beta)} + \frac{\eta G^2}{1-\beta}(2\sqrt{T}-1) + \frac{D^2}{2(1-\beta)} \sum_{t=1}^T \frac{\beta_t^2}{\eta_t}$$

■

Proof of Corollary 2.1 Proof Since $\beta_t = \beta\lambda^{t-1}$, by sum of arithmeticogeometric series we have

$$\sum_{t=1}^T \lambda^{2(t-1)}\sqrt{t} \leq \sum_{t=1}^T \lambda^{2(t-1)}t \leq \frac{1}{(1-\lambda^2)^2} \quad (23)$$

Plugging (23) into (22), we have

$$R_T \leq \frac{\sqrt{T}D^2\|D_T\|_1}{2\eta(1-\beta)} + \frac{\eta G^2}{1-\beta}(2\sqrt{T}-1) + \frac{D^2\beta^2}{2\eta(1-\beta)(1-\lambda^2)^2}.$$

■

B.2 Convergence Analysis in Nonconvex Stochastic Optimization

To prove Theorem 3 in §3.5, we first describe the Theorem 3.1 in (Chen et al., 2019):

Theorem 3.1 (Chen et al., 2019) For an Adam-type method under the assumptions:

- f is lower bounded and differentiable; $\|\nabla f(\theta) - \nabla f(\theta')\|_2 \leq L\|\theta - \theta'\|_2, \forall \theta, \theta'$.
- Both the true and stochastic gradient are bounded, i.e. $\|\nabla f(\theta_t)\|_2 \leq H, \|g_t\|_2 \leq H, \forall t$.
- Unbiased and independent noise in g_t , i.e. $g_t = \nabla f(\theta_t) + \zeta_t, \mathbb{E}[\zeta_t] = 0$, and $\zeta_i \perp \zeta_j, \forall i \neq j$.

Assume $\beta_t \leq \beta \leq 1$ in non-increasing, $\|\eta_t m_t / \sqrt{v_t}\|_2 \leq G$, then:

$$\begin{aligned} & \mathbb{E} \left[\sum_{t=1}^T \eta_t \langle \nabla f(\theta_t), \nabla f(\theta_t) / \sqrt{v_t} \rangle \right] \\ & \leq \mathbb{E} \left[C_1 \sum_{t=1}^T \left\| \frac{\eta_t g_t}{\sqrt{v_t}} \right\|_2^2 + C_2 \sum_{t=2}^T \left\| \frac{\eta_t}{\sqrt{v_t}} - \frac{\eta_{t-1}}{\sqrt{v_{t-1}}} \right\|_1 + C_3 \sum_{t=2}^{T-1} \left\| \frac{\eta_t}{\sqrt{v_t}} - \frac{\eta_{t-1}}{\sqrt{v_{t-1}}} \right\|_2^2 \right] + C_4 \quad (24) \end{aligned}$$

where C_1, C_2, C_3 are constants independent of d and T , C_4 is a constant independent of T , the expectation is taken w.r.t all the randomness corresponding to $\{g_t\}$.

Since APOLLO belongs to the family of *generalized Adam* (Chen et al., 2019) with $\sqrt{v_t}$ corresponding to D_t , we have

$$\begin{aligned} & \mathbb{E} \left[\sum_{t=1}^T \eta_t \langle \nabla f(\theta_t), \nabla f(\theta_t) / D_t \rangle \right] \\ & \leq \mathbb{E} \left[C_1 \sum_{t=1}^T \left\| \frac{\eta_t g_t}{D_t} \right\|_2^2 + C_2 \sum_{t=2}^T \left\| \frac{\eta_t}{D_t} - \frac{\eta_{t-1}}{D_{t-1}} \right\|_1 + C_3 \sum_{t=2}^{T-1} \left\| \frac{\eta_t}{D_t} - \frac{\eta_{t-1}}{D_{t-1}} \right\|_2^2 \right] + C_4 \quad (25) \end{aligned}$$

Note that APOLLO does not specify the bound of each update $\|\eta_t m_t / D_t\|_2$, because it is straight-forward to derive the bound with conditions $\eta_t \leq \eta, \|g_t\|_2 \leq H$ and $D_t \geq 1$.

Proof of Theorem 3 With (25), we can prove our Theorem 3 with similar derivations in Chen et al. (2019).

Proof We first bound non-constant terms in RHS of (25), which is given by

$$\mathbb{E} \left[C_1 \sum_{t=1}^T \left\| \frac{\eta_t g_t}{D_t} \right\|_2^2 + C_2 \sum_{t=2}^T \left\| \frac{\eta_t}{D_t} - \frac{\eta_{t-1}}{D_{t-1}} \right\|_1 + C_3 \sum_{t=2}^{T-1} \left\| \frac{\eta_t}{D_t} - \frac{\eta_{t-1}}{D_{t-1}} \right\|_2^2 \right]$$

For the term with C_1 , since $D_t \geq 1$, we have

$$\begin{aligned} \mathbb{E} \left[\sum_{t=1}^T \left\| \frac{\eta_t g_t}{D_t} \right\|_2^2 \right] &\leq \mathbb{E} \left[\sum_{t=1}^T \|\eta_t g_t\|_2^2 \right] \\ &= \mathbb{E} \left[\sum_{t=1}^T \left\| \left(\frac{\eta}{\sqrt{t}} \right) g_t \right\|_2^2 \right] \\ &\leq \eta^2 H^2 \sum_{t=1}^T \frac{1}{t} \leq \eta^2 H^2 (1 + \log T) \end{aligned} \tag{26}$$

where the last inequality is due to $\sum_{t=1}^T 1/t \leq 1 + \log T$.

For the term with C_2 , we have

$$\begin{aligned} \mathbb{E} \left[\sum_{t=2}^T \left\| \frac{\eta_t}{D_t} - \frac{\eta_{t-1}}{D_{t-1}} \right\|_1 \right] &= \mathbb{E} \left[\sum_{j=1}^d \sum_{t=2}^T \left(\frac{\eta_{t-1}}{D_{t-1,j}} - \frac{\eta_t}{D_{t,j}} \right) \right] \\ &= \mathbb{E} \left[\sum_{j=1}^d \left(\frac{\eta_1}{D_{1,j}} - \frac{\eta_T}{D_{T,j}} \right) \right] = \mathbb{E} \left[\sum_{j=1}^d \frac{\eta_1}{D_{1,j}} \right] \leq d\eta \end{aligned} \tag{27}$$

where the first equality is due to $\frac{D_{t-1,j}}{\eta_{t-1}} \leq \frac{D_{t,j}}{\eta_t}$, $\forall t \in [T], j \in [d]$ and the second equality is due to telescope sum.

For the term with C_3 , we have

$$\mathbb{E} \left[\sum_{t=2}^{T-1} \left\| \frac{\eta_t}{D_t} - \frac{\eta_{t-1}}{D_{t-1}} \right\|_2^2 \right] \leq \mathbb{E} \left[\eta \sum_{t=2}^{T-1} \left\| \frac{\eta_t}{D_t} - \frac{\eta_{t-1}}{D_{t-1}} \right\|_1 \right] \leq d\eta^2 \tag{28}$$

where the first inequality is due to $|\eta_{t-1}/D_{t-1,j} - \eta_t/D_{t,j}| \leq \eta$.

Then for APOLLO we have

$$\begin{aligned} \mathbb{E} \left[C_1 \sum_{t=1}^T \left\| \frac{\eta_t g_t}{D_t} \right\|_2^2 + C_2 \sum_{t=2}^T \left\| \frac{\eta_t}{D_t} - \frac{\eta_{t-1}}{D_{t-1}} \right\|_1 + C_3 \sum_{t=2}^{T-1} \left\| \frac{\eta_t}{D_t} - \frac{\eta_{t-1}}{D_{t-1}} \right\|_2^2 \right] + C_4 \\ \leq C_1 \eta^2 H^2 (1 + \log T) + C_2 d\eta + C_3 d\eta^2 + C_4 \end{aligned} \tag{29}$$

Now we lower bound the LHS of (25). With the assumption $\|D_t\|_\infty \leq L$, we have

$$(\eta_t/D_t)_j \geq \frac{\eta}{L\sqrt{t}}$$

And thus

$$\mathbb{E} \left[\sum_{t=1}^T \eta_t \langle \nabla f(\theta_t), \nabla f(\theta_t)/D_t \rangle \right] \geq \mathbb{E} \left[\sum_{t=1}^T \frac{\eta}{L\sqrt{t}} \|\nabla f(\theta_t)\|_2^2 \right] \geq \frac{\sqrt{T}}{L} \min_{t \in [T]} \mathbb{E} [\|\nabla f(\theta_t)\|_2^2] \quad (30)$$

Then, to sum up with (25), (29) and (30), we have

$$\frac{\sqrt{T}}{L} \min_{t \in [T]} \mathbb{E} [\|\nabla f(\theta_t)\|_2^2] \leq C_1 \eta^2 H^2 (1 + \log T) + C_2 d\eta + C_3 d\eta^2 + C_4$$

which is equivalent to

$$\begin{aligned} \min_{t \in [T]} \mathbb{E} [\|\nabla f(\theta_t)\|_2^2] &\leq \frac{L}{\sqrt{T}} (C_1 \eta^2 H^2 (1 + \log T) + C_2 d\eta + C_3 d\eta^2 + C_4) \\ &= \frac{1}{\sqrt{T}} (Q_1 + Q_2 \log T) \end{aligned}$$

This completes the proof. ■

Appendix C. APOLLO with Decoupled Weight Decay

Algorithm 2: APOLLO with weight decay (L_2 /Decoupled)

```

Initial:  $m_0, d_0, B_0 \leftarrow 0, 0, 0$  // Initialize  $m_0, d_0, B_0$  to zero
while  $t \in \{0, \dots, T\}$  do
  for  $\theta \in \{\theta^1, \dots, \theta^L\}$  do
     $g_{t+1} \leftarrow \nabla f_t(\theta_t) + \gamma \theta_t$  // Calculate gradient at step  $t$ 
     $m_{t+1} \leftarrow \frac{\beta(1-\beta^t)}{1-\beta^{t+1}} m_t + \frac{1-\beta}{1-\beta^{t+1}} g_{t+1}$  // Update bias-corrected moving
     $\alpha \leftarrow \frac{d_t^T (m_{t+1} - m_t) + d_t^T B_t d_t}{(\|d_t\|_4 + \epsilon)^4}$  // Calculate coefficient of  $B$  update
     $B_{t+1} \leftarrow B_t - \alpha \cdot \text{Diag}(d_t^2)$  // Update diagonal Hessian
     $D_{t+1} \leftarrow \text{rectify}(B_{t+1}, 1)$  // Handle nonconvexity
     $d_{t+1} \leftarrow D_{t+1}^{-1} m_{t+1} + \gamma \theta_t$  // Calculate update direction
     $\theta_{t+1} \leftarrow \theta_t - \eta_{t+1} d_{t+1}$  // Update parameters
  end
end
return  $\theta_T$ 

```

Algorithm 2 illustrates the algorithm of APOLLO with the standard L_2 and the decoupled weight decay. As APOLLO memorizes the update direction of the last iteration d_t to update the diagonal Hessian B_{t+1} , the application of decoupled weight decay to APOLLO is slightly different from AdamW. The weight decay term is added to the update direction d_t , instead of directly to the update of parameters. We conducted experiments to evaluate APOLLO with decoupled weight decay on image classification tasks. The results are provided in Appendix E.

Table 4: Hyper-parameters of each optimizer on CIFAR-10 and ImageNet.

	CIFAR-10	ImageNet
SGD	$\eta = 0.1, \gamma = 5e^{-4},$	$\eta = 0.1, \gamma = 1e^{-4}$
Adam	$\eta = 0.001, \gamma = 2.5e^{-1}, \epsilon = 1e^{-8}$	$\eta = 0.001, \gamma = 1e^{-1}, \epsilon = 1e^{-8}$
RAdam	$\eta = 0.001, \gamma = 2.5e^{-1}, \epsilon = 1e^{-8}$	$\eta = 0.001, \gamma = 1e^{-1}, \epsilon = 1e^{-8}$
AdaBelief.	$\eta = 0.001, \gamma = 2.5e^{-1}, \epsilon = 1e^{-8}$	$\eta = 0.001, \gamma = 1e^{-1}, \epsilon = 1e^{-8}$
AdaHessian	$\eta = 0.15, \gamma = 1e^{-3}, \epsilon = 1e^{-2}$	—
APOLLO	$\eta = 1.0, \gamma = 2.5e^{-4}, \epsilon = 1e^{-4},$	$\eta = 1.0, \gamma = 1e^{-4}, \epsilon = 1e^{-4}$
APOLLOW	$\eta = 1.0, \gamma = 2.5e^{-4}, \epsilon = 1e^{-4},$	$\eta = 1.0, \gamma = 1e^{-4}, \epsilon = 1e^{-4}$

Appendix D. Experimental Details

D.1 Image Classification

CIFAR-10 For CIFAR-10 dataset, we use the ResNet-110 architecture in the public implementation⁴. Note that ResNet-110 is a modified version of ResNet-18 (He et al., 2016) to adapt the small image size 32×32 in CIFAR-10, and is much smaller than standard ResNet-18. The number of parameters for ResNet-110 and ResNet-18 are 1.73 M and 11.69 M, respectively. The implementation of AdaHessian is based on the public implementation⁵. The training batch size is set to 128. For each optimizer, we used two learning rate decay strategies. First, we train the model on CIFAR-10 for 164 epochs and decay the learning rate at the end of 80-th and 120-th epochs by 0.1. Second, we also used the cosine annealing schedule (Loshchilov and Hutter, 2017). For the cosine annealing schedule, we train a CIFAR-10 model for 200 epochs.

For every optimizer, we comprehensively tuned its hyper-parameters and selected the set of hyper-parameters with the optimal classification accuracy. Concretely, for SGD, we fixed momentum at 0.9 and perform grid search of learning rate $\eta \in \{0.05, 0.1, 0.2, 0.5\}$, weight decay rate $\gamma \in [1e^{-4}, 1e^{-3}]$ with step $1e^{-4}$. For Adam and RAdam, we fixed $\beta_1 = 0.9, \beta_2 = 0.999, \epsilon = 1e^{-8}$ and grid search learning rate $\eta \in \{1e^{-4}, 5e^{-4}, 1e^{-3}, 5e^{-3}, 1e^{-2}\}$, weight decay rate $\gamma \in [1e^{-2}, 5e^{-1}]$ with step $1e^{-2}$. For AdaBelief, we fixed $\beta_1 = 0.9, \beta_2 = 0.999$, and grid search learning rate $\eta \in \{1e^{-4}, 5e^{-4}, 1e^{-3}, 5e^{-3}, 1e^{-2}\}$, and $\epsilon \in \{1e^{-6}, 1e^{-8}, 1e^{-12}\}$. For weight decay, we tried both the standard L_2 and the decoupled version of weight decay. For L_2 , we search weight decay rate $\gamma \in [1e^{-4}, 1e^{-3}]$ with step $1e^{-4}$, and for decoupled version we search weight decay rate $\gamma \in [1e^{-2}, 5e^{-1}]$ with step $1e^{-2}$. For AdaHessian, we fixed $\beta_1 = 0.9, \beta_2 = 0.999$ and grid search $\eta \in \{0.05, 0.1, 0.15, 0.2\}$, weight decay rate $\gamma \in [5e^{-4}, 5e^{-3}]$ with step $5e^{-4}$ and $\epsilon \in \{1e^{-2}, 1e^{-4}, 1e^{-6}\}$. For APOLLO, we fixed $\beta = 0.9, \epsilon = 1e^{-4}$ and grid search learning rate $\eta \in \{0.1, 0.5, 1.0, 2.0\}$, weight decay rate $\gamma \in [5e^{-5}, 1e^{-3}]$ with step $5e^{-5}$. We explored applying learning rate warmup to all the optimizers and found that APOLLO and AdaHessian significantly benefit from warmup. The impact of warmup on other optimizers is marginal. Thus, for APOLLO and AdaHessian,

4. <https://github.com/bearpaw/pytorch-classification>

5. <https://github.com/davda54/ada-hessian>

learning rates are warmed up linearly in the first 200 updates. The selected optimal hyper-parameters for each optimizer are summarized in Table 4 Random cropping and random horizontal flipping are applied to training data. For each experiment, we conduct training on one NVIDIA Tesla V100 GPU.

ImageNet For ImageNet, we used the neural architecture of ResNeXt-50 (Xie et al., 2017), with training batch size 256. For each optimizer, we also used the two learning rate decay strategies — milestone and cosine. For milestone decay, we train the model for 120 epochs and decay the learning rate at the end of 40-th and 80-th epochs by 0.1. For cosine annealing, we also train each model for 120 epochs with the cosine annealing schedule. For each optimizer, we fixed all the hyper-parameters selected from CIFAR-10 experiments, except the rate of weight decay γ which is tuned on the classification accuracy. Random cropping and random horizontal flipping are applied to training data. For each experiment, we conduct training on eight NVIDIA Tesla V100 GPUs.

D.2 Language Modeling

One Billion Words dataset (Chelba et al., 2013) is a publicly available benchmark for measuring progress of language modeling. It contains about 0.8 billion tokens with a vocabulary of 793,471 words, including sentence boundary markers. Different from Liu et al. (2020) which shrinks the vocabulary to about 0.64 million words, we used the standard vocabulary⁶. For the language model, we used two-layer LSTM with 2048 hidden states with adaptive softmax and 300-dimensional word embeddings as input. The cut-offs of the adaptive softmax are set to [60000, 100000, 640000], which is different from Liu et al. (2020). Dropout (Srivastava et al., 2014) is applied to each layer with drop rate of 0.1. No weight decay is applied to these optimizers. Gradient clips with 1.0 are applied to all the optimization methods.

For each optimizer, we comprehensively tuned its learning rate. Concretely, for SGD, we searched the learning rate $\eta \in \{0.05, 0.1, 0.5, 1.0\}$ and $\eta = 0.5$ was selected. For Adam, RAdam and AdaBelief, we fixed $\beta_1 = 0.9$, $\beta_2 = 0.999$, and searched for $\eta \in \{5e^{-4}, 1e^{-3}, 2e^{-3}, 5e^{-3}\}$, and finally $\eta = 1e^{-3}$ was selected. In addition, following Zhuang et al. (2020), we also tuned ϵ for AdaBelief (for Adam and RAdam, we fixed $\epsilon = 1e^{-8}$). We searched $\epsilon \in \{1e^{-8}, 1e^{-12}, 1e^{-16}\}$ and found that $\epsilon = 1e^{-12}$ worked best. It should be noticed that AdaBelief is very sensitive to the value of ϵ . The result in Table 2 is obtained using $\epsilon = 1e^{-12}$. With other values, e.g. $1e^{-8}$ or $1e^{-16}$, the PPL points of AdaBelief are even higher than Adam and RAdam. Thus, we suspected that the improvement of AdaBelief over Adam or RAdam on LSTM mainly comes from the fine-tuning of ϵ . Similar observations were also found in our experiments of image classification, and were reported in Yuan and Gao (2020). For APOLLO, we fixed $\beta = 0.9$, $\epsilon = 1e^{-4}$, and searched $\eta \in \{1.0, 5.0, 10.0\}$. Finally, $\eta = 10.0$ was selected. Each model is trained for 20 epochs, and the learning rate decays at the end of the 12-th and 18-th epochs by decay rate 0.1. LSTMs are unrolled for 20 steps without resetting the LSTM states and the batch size is set to 128. Every models is trained on one NVIDIA Titan RTX GPU.

6. https://github.com/rafaljozefowicz/lm/blob/master/1b_word_vocab.txt

D.3 Neural Machine Translation

Our experiments on WMT 2014 English-German are based on the Transformer-base model (Vaswani et al., 2017), with implementation from the FairSeq package (Ott et al., 2019). This dataset contains 4.5M parallel sentence pairs for training. We follow the standard setting (Vaswani et al., 2017), using Newstest2013 as the validation set and Newstest2014 as the test set. The dataset is pre-processed following (Ma et al., 2019), using the scripts from FairSeq package⁷. Specifically, we use word embedding with 512 dimension and 6-layer encoder/decoder with 8 multi-head attention and 2048 feed-forward dimensions. We apply 0.1 label smoothing (Szegedy et al., 2016), and perform totally 500,000 updates to train each model. For Adam, RAdam and AdaBelief, we use start learning rate 0.0005. For Adam we set $\beta = (0.9, 0.98)$, while for RAdam and AdaBelief we set $\beta = (0.9, 0.999)$. For SGD and APOLLO, the start learning rates is 0.1 and 10.0, respectively. The momentum of SGD is 0.9. For learning rate scheduling, we applied linear warm up the learning rate for SGD, Adam, AdaBelief, and APOLLO — 4000 updates for Adam and 1000 updates for SGD, AdaBelief and APOLLO. For RAdam, we did not apply warm up because RAdam is inherently designed to avoid it. After learning rate warming up, we applied the inverse square root decay (Vaswani et al., 2017) to Adam. For SGD, RAdam, AdaBelief and APOLLO, we decayed the learning rate at the 250,000 and 450,000 updates by decay rate 0.1. Gradient clips with 1.0 are applied to all the optimization methods, and the dropout ratio are set to 0.1. Weight decay rates are $1e^{-4}$ for Adam-type methods, $1e^{-6}$ for SGD, and $1e^{-8}$ for APOLLO. The decoding beam size is set to 5, and the checkpoints of the last 10 epochs are averaged before evaluation. For each experiment, we conducted distributed training across eight NVIDIA Tesla V100 GPUs with maximum batch size as 8192 tokens per GPU (totally 8192×8 tokens per batch).

Appendix E. Detailed Experimental Results

In this section, we report the detailed experimental results in Section 4, and the results of investigation of the effect of weight decay.

E.1 Detailed Results on Image Classification

Figure 4 and Table 5 illustrate the details of the experimental results on Image Classification. For each experiment, we report the mean values with corresponding standard deviations over 5 runs. Though Loshchilov and Hutter (2019) claimed that the optimal settings of the learning rate and weight decay factor in Adam with decoupled weight decay is more independent than the original Adam, we observed that the strength of weight decay regularization is still co-related with the learning rate. To illustrate the significant effect of weight decay strength on both the performance of convergence and generalization, we also report the performance of Adam and RAdam with the same weight decay rate of SGD, named Adam* and RAdam*.

From Figure 4 and Table 5, we see that Adam* and RAdam*, with the same weight decay rate of SGD, converge much faster than other optimization methods, while obtaining significantly worse classification accuracy. After adjusting the weight decay rates, the test accuracy of Adam and RAdam remarkably improves, with rapid decline of convergence speed. This suggests that the fast convergence speed of Adam and RAdam results from relatively

7. <https://github.com/pytorch/fairseq>

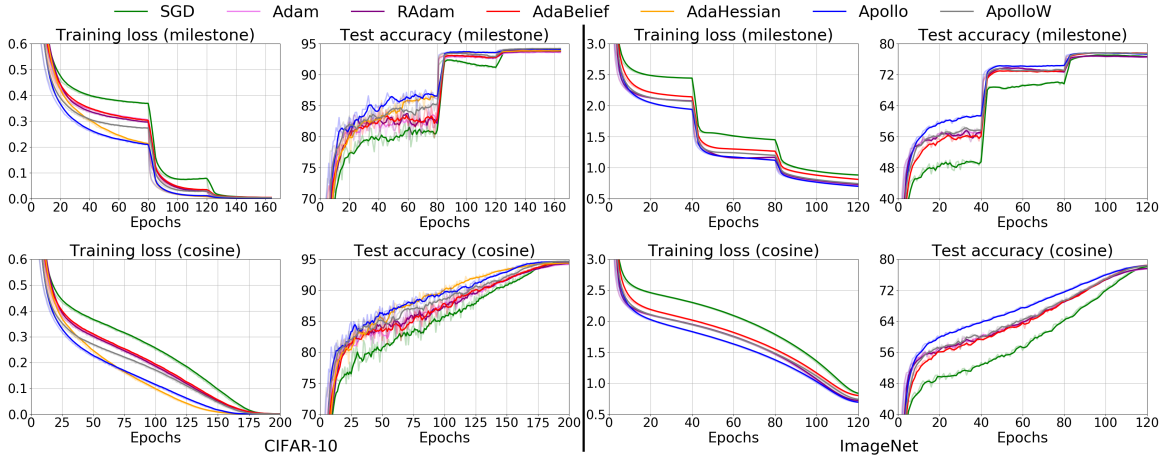


Figure 4: Training loss and test accuracy of ResNet-110 on CIFAR-10 and ResNeXt-50 on ImageNet, with two schedule strategies of learning rate decay.

Table 5: Classification accuracy on CIFAR-10 and ImageNet. For each experiment, we report the mean and standard variance over 5 runs.

Method	CIFAR-10		ImageNet	
	milestone decay	cosine annealing	milestone decay	cosine annealing
SGD	93.94±0.07	94.53±0.27	77.57±0.07	78.26±0.08
Adam*	91.41±0.30	91.56±0.19	71.72±0.13	71.19±0.10
RAdam*	91.80±0.04	91.88±0.15	72.37±0.08	71.64±0.14
Adam	93.74±0.15	94.24±0.09	76.86±0.06	77.54±0.16
RAdam	93.88±0.11	94.38±0.25	76.91±0.07	77.68±0.08
AdaBelief	94.03±0.11	94.51±0.07	77.55±0.08	78.22±0.11
AdaHessian	93.97±0.22	94.48±0.17	—	—
APOLLO	94.21±0.08	94.64±0.09	77.85±0.07	78.45±0.06
APOLLOW	94.34±0.12	94.76±0.07	77.86±0.09	78.48±0.07

weak regularization. Thus, the effect of regularization strength needs to be considered when we analyze the performance of different optimization methods.

In addition, we also report the results of APOLLO with decoupled weight decay, which is denoted as APOLLOW. The hyper-parameters of APOLLOW (see Table 4) are exactly the same of the optimal ones of APOLLO. From Figure 4 and Table 5, we see that APOLLO with the standard L_2 regularization achieves faster convergence speed, while APOLLOW with the decoupled weight decay achieves slightly better generalization accuracy. Importantly, comparing with Adam-type methods whose performance is significantly impacted by different weight decay implementations, APOLLO is much more consistent with the two implementations of weight decay.

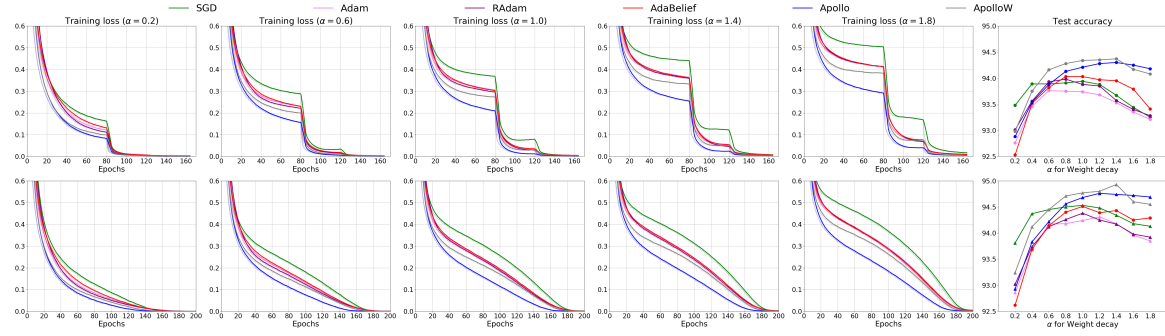


Figure 5: Training loss and test accuracy of ResNet-110 on CIFAR-10 with various rates of weight decay, with two schedule strategies of learning rate decay.

E.2 Effect of Weight Decay Rate on Optimization

To further investigate the effect of weight decay rate on converge speed and generalization performance for different optimization methods, we conduct experiments on CIFAR-10 of ResNet-110 with a range of weight decay rates. Concretely, we use the weight decay rates γ in Table 4 as the base, and explore different γ that are α times of the base weight decay rate, with $\alpha \in \{0.2, 0.6, 1.0, 1.4, 1.8\}$.

Figure 5 shows the convergence of different optimization methods with various rates of weight decay, together with the classification accuracy. APOLLO achieves improvements over all the four baselines on convergence speed with different rates of weight decay. For classification accuracy, APOLLO obtains the best accuracy when the weight decay rate ratio α is larger than 0.3. When the weight decay rate is decreasing, SGD obtains the best accuracy, while APOLLO achieves comparable performance.

E.3 Comparison on Training Speed and Memory Cost

In this section, we compare the training speed and memory between SGD, Adam, AdaHessian and APOLLO. Table 6 summarizes the comparison of cost of a single iteration of update. Note that the cost measured in our experiments includes all aspects of model training, including the forward and backward pass of DNNs, not only that of updating parameters for an optimizer. For fair comparison, experiments of CIFAR-10 and One Billion Words are conducted on a single NVIDIA TITAN RTX GPU, while experiments of ImageNet and WMT are performed with distributed training on 8 NVIDIA Tesla V100 GPUs.

Table 6: Comparison between different optimization methods on training speed and memory cost. Cost includes all aspects of model training, not only that of an optimizer.

Cost (\times SGD)	CIFAR-10		ImageNet		1BW		WMT-14	
	Speed	Memory	Speed	Memory	Speed	Memory	Speed	Memory
SGD	1.00	1.00	1.00	1.00	1.00	1.00	1.00	1.00
Adam	1.16	1.01	1.01	1.03	1.19	1.34	1.13	1.04
Apollo	1.42	1.01	1.23	1.05	1.49	1.62	1.19	1.06
AdaHessian	5.76	2.12	11.78	2.51	3.51	2.78	8.46	2.47

From Table 6, we see that the second-order AdaHessian requires much more computational resource than first-order methods on both time and memory. In addition, the slow-down of AdaHessian becomes more significant for larger-scale models with distributed training across multiple GPUS, such as ResNext-50 on ImageNet and Transformer on WMT.

E.4 Experiments on Parameter-Wise Gradient Clipping

In this section, we provide some preliminary results on parameter-wise gradient clipping, a modification of the standard gradient clipping that is inherently proper to APOLLO. Parameter-wise gradient clipping is to clip the gradient of each parameter individually based on its own norm. It can be regarded as a trade-off between gradient clipping by global norm and by each value.

We conducted two groups of experiments to compare with the standard gradient clipping method — language modeling and neural machine translation. The experimental settings for standard gradient clipping are exactly the same as in section 4, where we clipped the gradient by global norm 1.0 for each model. For parameter-wise gradient clipping, we clipped each parameter by 0.5 for the LSTM model in language modeling, and 0.1 for the Transformer-base model in NMT.

Table 7: Comparison between APOLLO with standard and parameter-wise gradient clipping on One Billion Words and WMT-14. We report the mean and standard variance over 5 runs.

	1BW	WMT-14
Standard	31.94 ± 0.09	28.34 ± 0.10
Parameter-wise	31.75 ± 0.10	28.39 ± 0.11

Table 7 lists the preliminary results. On both the two groups of experiments, parameter-wise gradient clipping slightly outperforms the standard one.

Appendix F. Experiments with Small Toy CNN Models

In this section, we provide the comparison between SdLBFGS (Wang et al., 2017) and APOLLO on CIFAR-10 dataset with a small toy CNN model⁸. The implementation of SdLBFGS is based on the public PyTorch release⁹, which includes two important modifications to the original SdLBFGS algorithm: identity matrix initialization and direction normalization (Li and Liu, 2018). For each optimizer, we train the CNN model for 50 epochs with batch size equals to 64. After each epoch, the learning rate is decayed by the rate 0.95. For the start learning rate for each optimizer, we performed search in a wide range: $\eta \in \{1.0, 0.5, 0.2, 0.1, 0.05, 0.01, 0.005\}$, and select the one obtains the optimal performance. The final start learning rate for both SdLBFGS and APOLLO is 0.1. Following Li and Liu (2018), the memory size of SdLBFGS is set to 100. For APOLLO, we linearly warmed up the learning rate from 0.01 in the first 10 updates. For other hyper-parameters of each optimizer, we choose the default value.

8. https://pytorch.org/tutorials/beginner/blitz/cifar10_tutorial.html

9. <https://github.com/harryliew/SdLBFGS>

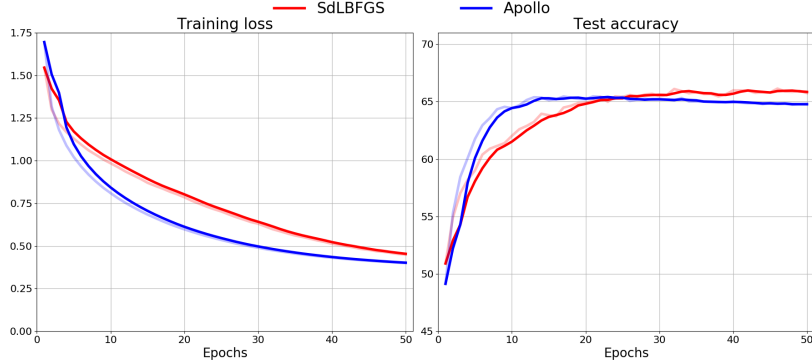


Figure 6: Training loss and test accuracy of SdLBFGS and APOLLO on CIFAR-10 with the small toy CNN model.

From Figure 6, we see that APOLLO converges faster than SdLBFGS and obtains comparable test accuracy. Note that APOLLO is much faster (more than 10 times for one iteration) than SdLBFGS and consumes much less memory (SdLBFGS stores 100 previous update directions).

Appendix G. Scale-Invariant Apollo

In (11), we rectify the absolute value of B_t with a convexity hyper-parameter σ :

$$D_t = \text{rectify}(B_t, \sigma) = \max(|B_t|, \sigma)$$

To make APOLLO scale-invariant, we modify this rectification operation by incorporating a term similar to the gradient ‘‘belief’’ (Zhuang et al., 2020):

$$D_t = \text{rectify}(B_t, \sigma) = \max(|B_t|, \sigma \|g_{t+1} - g_t\|_\infty) \quad (31)$$

It is not hard to prove that APOLLO with the rectification in (31) is scale-invariant. Importantly, after this modification, σ is still coupled with the stepsize η , and we can set $\sigma = 1$ in practice. Thus, we do not introduce new hyper-parameters.